White Paper: *Kepler* **Microlens Planets and Parallaxes**

Andrew Gould[1] **& Keith Horne**[2]

Executive Summary

In its first 4 years, *Kepler* discovered thousands of hot planets, including many small ones, that transit their host stars. With 2 reaction wheels, *Kepler* can no longer deliver the μmag photometry required for transit surveys, but rather mmag photometry over its 115 deg^2 field of view. By pointing toward Baade's window, *Kepler* can observe hundreds of Galactic Bulge microlensing event lightcurves *simultaneously*, with near-continuous coverage and from a perspective displaced from the Earth by 0.15-0.4 AU (projected). *Kepler* will then see microlens lightcurves offset in time and in peak magnification relative to those from Earth, determining the distance and mass of the lens stars and their planets. *Kepler*'s lightcurves also probe for planets along different image trajectories on the lens plane, potentially more than doubling the number of detectable microlens planets. Pointing constraints, as we understand them, limit *Kepler*'s coverage to two 14-day windows in Spring and two more in Fall of each year. We show that microlens parallaxes can still be uniquely measured for of order 300 events that peak near one of the two Spring windows.

1 Introduction

Although not at all designed for this purpose, *Kepler* could have operated as a superb microlensing parallax satellite as it was originally constructed. It would have returned high-quality "microlens parallaxes" for over half of all the 2000 microlensing events that are discovered each year toward the Galactic Bulge, including about 3/4 of the events containing exo-planets. For these exo-planet events, the microlens parallax nearly always permits measurement of the mass and distance of the lens (and its planet). Such mass/distance measurements enormously increase the value of microlensing planets, since without them only the planet-star mass ratio is known, while the distance is at best weakly constrained. Hence such measurements would enable much more precise characterization of individual systems and would also allow determination of the Galactic distribution of planets. Microlensing is primarily sensitive to planets somewhat beyond the snow line, where other techniques either fail completely or are sensitive only to giant planets. Hence, these mass/distance determinations would greatly enrich our understanding of a region of parameter space that is not readily accessible to other techniques.

In its present condition, *Kepler* retains significant microlensing capabilities. The principal challenge posed by the reaction wheel failures is that *Kepler* can point at the microlensing target fields for only two 14-day periods during the microlensing season. This compares to 107 continuous days (over half the season including the richest part) if it had 3 functioning reaction wheels. By contrast, the problems with pointing stability and jitter have relatively little impact on *Kepler*'s microlensing performance.

The key feature of *Kepler* for microlensing remains intact: capability to *simultaneously* observe essentially all ongoing microlensing events. This enables good integrated signal-to-noise ratio (S/N) despite large pixel size (and therefore relatively high background in crowded Bulge fields). Its unique perspective also permits *Kepler* to independently discover planets in these events, since *Kepler*'s lightcurves probe regions on the lens plane displaced from those probed by lightcurves from Earth.

A *Kepler* microlensing program could therefore both (1) return excellent science and (2) serve as a pathfinder mission. It is true that the shortened observing windows substantially reduce the

[1]Department of Astronomy, Ohio State University, 140 W. 18th Ave., Columbus, OH 43210, USA; gould@astronomy.ohio-state.edu

[2]SUPA, University of St Andrews, School of Physics & Astronomy, North Haugh, St Andrews, KY16 9SS, Scotland, UK; kdh1@st-and.ac.uk

number of microlens parallaxes and planet masses. However, this would still be a major advance on what is possible from the ground. But of equal importance, such a program would test a *Kepler*-like microlensing mission in practice. A future dedicated mission built on this experience could revolutionize microlensing in the upcoming era of massive microlensing planet searches, including *WFIRST*.

We also note that there are opportunities for substantial synergy with *Spitzer*, which would be aided considerably if first observations could begin 15 April 2014.

2 Microlens Planets: A Brief Primer

Microlensing searches are currently detecting about 12 planets per year, and this number is likely to increase substantially in the near future with the ramp-up of new experiments. While these numbers are still small compared to the thousands of planets (and strong planetary candidates) detected by *Kepler* and other techniques, the microlensing planets lie in a unique region of parameter space, i.e., a factor ~ 2 beyond the snow line and down to Earth-like masses. Other techniques either do not probe this region at all, or do so only for giant planets. Hence, the cool planets detected by microlensing are complementary to the generally warmer planets found by *Kepler* and by radial velocities. Moreover, microlensing planets lie at a range of distances from the solar neighborhood to the Galactic Bulge, and therefore in principle permit measurement of the Galactic distribution of planets.

Why are microlensing planets typically just beyond the snow line? With or without planets, a lens star breaks up the source light into two magnified images. If one of these images passes close to a planet of the lens star, the planet further perturbs the image, giving rise to a microlensing lightcurve deviation. As the source gets closer to the projected position of the lens, the magnifications (and so image sizes) get bigger and closer to the Einstein ring, where they are most easily perturbed. Hence, microlensing is most sensitive to planets within a factor ~ 1.5 of the Einstein ring, which is at $r_{\rm E} = D_L\theta_{\rm E}$, where

$$\theta_{\rm E} = \sqrt{\kappa\, M\, \pi_{\rm rel}} \qquad \left(\kappa \equiv \frac{4\,G}{c^2\,{\rm AU}} \sim 8.1\,\frac{\rm mas}{M_\odot}\right) \tag{1}$$

is the angular Einstein radius, M is the lens mass, and $\pi_{\rm rel} = {\rm AU}\left(D_L^{-1} - D_S^{-1}\right)$ is the lens-source relative parallax. For typical distances $D_L \sim 4$ kpc to the lens and $D_S \sim 8$ kpc to the source, $r_{\rm E} \sim 3.5\,{\rm AU}(M/M_\odot)^{1/2}$. Since this is projected, the typical physical separation is $a \sim (3/2)^{3/2} r_{\rm E} \sim 4.3\,{\rm AU}(M/M_\odot)^{1/2}$. For comparison, the snow line is generally thought to scale as $r_{\rm snow} \sim 2.7\,{\rm AU}(M/M_\odot)$.

In the simplest case (Gould & Loeb 1992; Gaudi 2012), microlensing events require siz parameters: three for the underlying event $(t_{\rm E}, t_0, u_0)$ and three more for the planetary perturbation (s, q, α). The first three are just the Einstein timescale

$$t_{\rm E} = \frac{\theta_{\rm E}}{\mu_{\rm geo}} = 37\,{\rm day}\left(\frac{M}{0.5\,M_\odot}\right)^{1/2}\left(\frac{\pi_{\rm rel}}{40\mu{\rm as}}\right)^{1/2}\left(\frac{\mu_{\rm geo}}{4\,{\rm mas\,yr^{-1}}}\right)^{-1}, \tag{2}$$

the time of peak t_0, and the impact parameter (in units of $\theta_{\rm E}$) u_0. Here, $\mu_{\rm geo}$ is the lens-source relative proper motion (geocentric). The three planetary parameters are s (projected separation in units of $\theta_{\rm E}$), q (planet-star mass ratio), and α (lens-source trajectory direction relative to the planet-star separation). Hence, microlensing lightcurves typically determine only the mass ratio q, not the planet mass $m = q\,M$. And since the host is generally not seen in the glare of the source light, M is not generally known.

The situation is actually somewhat better than this because in nearly all planetary events, the source passes over or near caustic features due to the planet (otherwise the planet would not be detected). The structure of the lightcurve then depends on the ratio $\rho = \theta_*/\theta_{\rm E}$ of the source

size θ_* to $\theta_{\rm E}$. Since θ_* is routinely measured from the color and magnitude of the source (Yoo et al. 2004), planetary events almost always yield $\theta_{\rm E} = \theta_*/\rho$. Hence, they also yield the product $M\,\pi_{\rm rel} = \theta_{\rm E}^2/\kappa$ [Equation (1)]. However, to completely break the degeneracy (and so determine M and $\pi_{\rm rel}$ separately) requires one to measure the "microlens parallax", $\pi_{\rm E}$.

3 Why Microlens Parallaxes Are Crucial

Microlens parallaxes nail down the masses and distances of the lens stars and their planets. Simpler point-lens microlensing events are characterized by just three event parameters $(t_{\rm E}, t_0, u_0)$. Of these only $t_{\rm E}$ is related to the physical parameters of the system $(M, \pi_{\rm rel}, \mu_{\rm geo})$. See Equation (2). That is, two additional parameters must be measured if one is to determine M and $\pi_{\rm rel}$. (Since the source distance is generally known quite well, knowing $\pi_{\rm rel}$ is equivalent to knowing the lens distance D_L.)

But as just mentioned, planetary microlensing events routinely yield $\theta_{\rm E}$. Hence for these events, the "microlens parallax" $\boldsymbol{\pi}_{\rm E}$, which is the trigonometric parallax scaled to $\theta_{\rm E}$,

$$\pi_{\rm E} = \frac{\pi_{\rm rel}}{\theta_{\rm E}}; \qquad \frac{\boldsymbol{\pi}_{\rm E}}{\pi_{\rm E}} = \frac{\boldsymbol{\mu}_{\rm geo}}{\mu_{\rm geo}} \tag{3}$$

is especially important. That is, if $\theta_{\rm E}$ and $\pi_{\rm E}$ are both measured, then one directly obtains

$$M = \frac{\theta_{\rm E}}{\kappa\,\pi_{\rm E}}; \qquad \pi_{\rm rel} = \theta_{\rm E}\,\pi_{\rm E}. \tag{4}$$

4 How Microlens Parallaxes Are Measured From Space

Since *Kepler* is separated from Earth by a distance $\mathbf{d}_\perp$ (projected on the plane of the sky) it sees the microlensing events from a distinct perspective, peaking at a different time, and reaching a different peak magnification. From *Kepler*'s perspective, the lens-source separation will be different by an angle $\Delta\boldsymbol{\theta} = \pi_{\rm rel}\,\mathbf{d}_\perp/{\rm AU}$, displaced in the Einstein ring by

$$\Delta\mathbf{u} = \frac{\Delta\boldsymbol{\theta}}{\theta_{\rm E}} = \frac{\pi_{\rm rel}\,\mathbf{d}_\perp/{\rm AU}}{\theta_{\rm E}} = \pi_{\rm E}\frac{\mathbf{d}_\perp}{\rm AU}\ . \tag{5}$$

Kepler therefore sees the microlensing lightcurve with a different t_0 and a different u_0. Therefore, it at least appears relatively simple to find $\boldsymbol{\pi}_{\rm E}$ by comparing the values of t_0 and u_0 as measured on Earth and by *Kepler* :

$$\boldsymbol{\pi}_{\rm E} = \frac{\rm AU}{d_\perp}\,(\hat{\mathbf{x}}\,\Delta\tau, \hat{\mathbf{y}}\,\Delta\beta); \qquad \Delta\tau \equiv \frac{t_{0,{\rm Kep}} - t_{0,\oplus}}{t_{\rm E}}; \qquad \Delta\beta \equiv u_{0,{\rm Kep}} - u_{0,\oplus}, \tag{6}$$

where $\hat{\mathbf{x}}$, $\hat{\mathbf{y}}$ are the directions parallel and perpendicular to $\mathbf{d}_\perp$. In fact, there is some subtlety. The lightcurve magnification A depends only on the *square* of the lens-source normalized separation u: $A = A[u(t)]$, $u(t)^2 = u_0^2 + (t - t_0)^2/t_{\rm E}^2$, but u_0 is itself a signed quantity (depending on whether the lens passes the source on one side or the other). Hence, while the first component of $\boldsymbol{\pi}_{\rm E}$ is unambiguous, the second can take on any of four values: $+\Delta\beta_-, -\Delta\beta_-, +\Delta\beta_+, -\Delta\beta_+$. See Figure 1. The subscript refers to the source and lens being on the same $(-)$ or opposite $(+)$ side as seen from the two observers, while the sign to the left signifies that the lens passes the source on its right $(+)$ or left $(-)$ as seen from Earth. Fortunately we are interested primarily in the magnitude of $\pi_{\rm E}$ (hence of $\Delta\beta$) so this four-fold degeneracy reduces to a 2-fold degeneracy, $\Delta\beta_\pm$.

Nevertheless, since the two remaining solutions can yield quite different values of $\pi_{\rm E}$, it is important to distinguish them. This has been the subject of intensive study over the past 2 decades. Space constraints preclude a thorough discussion in this white paper (WP). We therefore simply list the main methods for doing this and give appropriate references. Satellite motion relative to Earth

yields different timescales $t_{\rm E}$ which permit breaking the $\Delta\beta$ degeneracy (Gould 1995; Boutreux & Gould 1996; Gaudi & Gould 1997). The accelerated motion of Earth can yield the component $\pi_{\rm E,\parallel}$ of $\boldsymbol{\pi}_{\rm E}$ that is parallel to this acceleration (Gould et al. 1994), which can be combined with the measured $\Delta\tau$ to extract the full $\boldsymbol{\pi}_{\rm E}$ (Gould 1999; Dong et al 2009b). For events with high magnification as seen from Earth, the degenerate solutions are quite close, so the degeneracy has no practical impact (Gould & Yee 2012). Further below we demonstrate by simulations that *Kepler* is fully capable of breaking the $\Delta\beta_\pm$ degeneracy in some representative cases. We show that it is also sometimes capable of breaking the $\pm\Delta\beta$ degeneracy but that even when it is not, this degeneracy does not significantly interfere with the mass measurement.

5 Kepler Microlensing Observations

Kepler can deliver near-continuous lightcurves for hundreds of microlens events observed in parallel over its wide field of view, but the pointing restrictions, as we understand them, limit coverage to two 2-week intervals in Spring and another two in Fall of each year. *Kepler* can observe fields near the ecliptic (including the Galactic Bulge microlens fields) only with the boresight at Sun-angles of $\pm45^\circ$ and $\pm90^\circ$, i.e., 4 times per orbit ($P = 372$ days). Because the field is approximately $\Delta\phi = 13.5^\circ$ across its principal axes, this actually means that any given point can be observed for about $P\,\Delta\phi/360^\circ \sim 14$ days near each of these four times. For the Galactic Bulge fields, these intervals in 2014–2015 are

$$1-14\,\text{Mar 2014};\quad 16-29\,\text{Apr 2014};\quad 28\,\text{Oct}-9\,\text{Nov 2014};\quad 13-25\,\text{Dec 2014};$$
$$9-21\,\text{Mar 2015};\quad 23\,\text{Apr}-6\,\text{May 2015};\quad 4-17\,\text{Nov 2015};\quad 21\,\text{Dec 2015}-3\,\text{Jan 2016}.$$

See Figure 2. It might be possible to extend these if the boresight does not have to be pointed *exactly* at these Sun-angles. For example, if the angle could actually be in the 10° interval $90^\circ \pm 5^\circ$, then *Kepler*'s observation windows could be expanded from 14 to 24 days. However, in this WP, we consider only 14-day intervals.

Parallax measurements require simultaneous observations from Earth, and these are impossible in Oct-Jan, so we focus on the Mar-May intervals. (However, "baseline" observations are actually needed and these can be done during a subset of the Oct-Jan intervals.)

The first intervals within the (Summer 2014+) framework of this program are Mar and Apr-May 2015. We focus on these. However, as we will comment in Section 7 below, an earlier interval of observations in Apr 2014 would be especially useful for synergy with *Spitzer*.

In our basic observing protocol, targets would be uploaded to *Kepler* on 8 Mar 2015, and again on 22 Apr 2015, i.e., just prior to the two intervals. These would then be observed continuously for the 14 days in each interval. Targets from the first interval would also be observed in the second, but of course new targets in the second interval would not be observed in the first.

We estimate that prior to 8 Mar 2015, the OGLE and MOA teams will have identified a total of 130 microlensing events that will peak after 1 Mar 2015, and so would be suitable for these observations. This estimate is based on 2013 data and takes into account that OGLE was still fine-tuning its system and so identified many events in outlying fields late, but will be more prompt in 2015. Similarly, we estimate 180 additional events identified by 22 Apr 2015 and peaking after 16 Apr 2015. Hence we can potentially monitor a total of 310 events or about 15% of all events. The expected number of planets contained within these events is therefore about 2, or perhaps somewhat higher due to the increasing rate of microlens planet discovery.

How many events can be observed simultaneously? We assume that we must download the full 1.4° arc (rather than moving arclets within the arc based on more aggressive software development). We assume full download capability of $(5.4\times10^6$ pixels$)\times$ (1440 epochs/long-cadence) and individual download arcs of $6\times1260\times90\% = 6800$ pixels, where the last factor accounts for gaps. We assume 5 minute exposures to minimize trailing and assume 14 days of observations per long-cadence

download. This allows 280 targets. Hence, plenty of excess capacity for the first 14 day of interval, and adequate capacity for the second (after eliminating events that have returned to baseline or are too faint to observe).

6 Crowding and Signal-to-Noise Ratio

Kepler photometry will be background-limited in the crowded Galactic Bulge fields. However, with near-continuous coverage, it will have somewhat better precision than ground-based microlens surveys, which will be sufficient to measure microlens parallaxes and independently probe for cool planets by virtue of its displaced perspective.

The target characteristics and performance requirement of a *Kepler* microlensing program differ quite radically from *Kepler*'s transit mission. Microlensing observations are directed toward the most optically crowded wide-angle fields in the Galaxy. The targets are mostly very faint ($I \gtrsim 16$) compared to typical transit-search targets ($V \lesssim 15$). Thus, even within one *Kepler* pixel, there are likely to be one or several other stars of comparable brightness to the target. On the other hand, as we show below, photometric precision of 0.05 mag per observation would yield highly precise microlens parallaxes (assuming that the photometric errors between measurements are uncorrelated). Thus, *Kepler*'s capacity to make these measurements must be thought through from the bottom up.

We first ask: what is the photometric precision assuming that the star field can be modeled perfectly. We assume 3700 photons per second at $I = 15$ (using the *Kepler* response function and the conservative example of a $T = 5800$K star with $E(V-I) = 2$). While conditions vary considerably, we adopt a mean "background" (overwhelmingly stars) of $I = 17.5\,\mathrm{mag\,arcsec^{-2}}$. Most targets will be relatively near the center of the *Kepler* field, where the PSF has a FWHM of $\theta_{\rm FWHM} = 3.1''$. In our proposed mode of 5 minute exposures, the images would be trailed by $\epsilon = 4.5''$. Hence, the effective background area in the oversampled limit is $(\pi/0.70 \ln 4)\,\theta^2_{\rm FWHM} = 30\,\mathrm{arcsec}^2$ (Gould & Yee 2013). Since a pixel is 2 times smaller than this number, the oversampled limit is too generous: we adopt $40\,\mathrm{arcsec}^2$. Hence, the background light is approximately $I = 13.5$, i.e., we are background limited in essentially all cases. This implies a photometric precision of $\sigma = 0.05 \times 10^{(I-18.4)/2.5}$ mag.

Can this precision be achieved in practice and will the errors be uncorrelated? There is good reason to believe that the answer to both questions is "yes". The distribution of background light will be measured at much higher ($\sim 1''$) resolution in V and I from intensive ground-based microlensing observations. Transforming these to unfiltered bands is known to work to better than 1% (Yee et al. 2012). The (typically 3–5) brighter sources in the PSF can be fit to very high precision using the ensemble of $\sim 2 \times 10^4$ measurements together with their precise positions and these initial 1% "guesses". The estimates can be used directly for the fainter sources. Note that 1% flux errors in these faint stars leads to errors in lensed-star photometry that are much smaller than 1% of the faint sources, because it is only *differences between images* that directly contributes to the error, not the *differences between background-model and reality*. The systematic errors in these measurements are small compared to 5%, so they do not impact the individual errors. However, if these systematic errors were the same in each measurement, they could not be "beat down as square-root of N". But these systematic errors come from intrapixel variations and flatfielding errors. Since the target lands on thousands of different pixels, and at random positions on each, such errors are effectively uncorrelated. Accounting for 10% loss due to the photometry arcs crossing CCD gaps, we estimate 260 images per day. Hence 0.05 mag errors (at $I = 18.4$ which is faint relative to typical targets) corresponds to errors of 0.003 mag per day.

We adopt these errors in for two examples shown in Figure 3. These correspond to typical lenses in the Galactic Disk and Bulge, respectively. Note that in 3 of the panels, we consider that the *Kepler* source flux is determined just from the overall fit. But in the last panel, we consider the impact of using the flux-alignment method of Yee et al. (2012), mentioned above. These examples

show that even with conservative estimates on the photometric precision, high-precision parallax measurements are possible.

7 Potential Synergy with Spitzer

Spitzer is also in an Earth-trailing orbit and so can also, in principle be used for microlens parallax measurements. Compared to *Kepler*, *Spitzer* has the advantages of 1) 38 day continuous observing window (instead of two widely separated 14 day windows), 2) Windows are currently in June-July, i.e., straddling the "peak" of the microlensing season (21 June ± 45 days), 3) Smaller PSF ($1''$ vs. $3''$) and pixel size ($1.2''$ vs. $4''$), 4) Non-trailed images.

These seem formidable, but *Kepler* also has two major advantages: 1) Observes all lensing events simultaneously (not sequentially), 2) Passband closer to SED peak of even heavily reddened sources.

Hence, *Kepler* and *Spitzer* present complementary opportunities for microlensing science, with different passbands and observing modes, and, most critically, complementary time coverage of the Galactic Bulge microlensing target fields.

In particular, we note that the examples shown in Figure 3 are events that peak in early March and then are reobserved by *Kepler* in April-May. The latter "second-epoch" observations are important for pinning down the microlens parallax. Now, *Kepler* itself cannot provide second-epoch observations for targets discovered and peaking in April-May. However, *Spitzer* could provide such a second-epoch because its window begins roughly 34 days after the second *Kepler* window ends.

This synergy can potentially be implemented in 2014. There is a Cycle-10 *Spitzer* proposal to observe microlensing events continuously from 2 June to 12 July 2014. While it is unknown at the time of this writing whether this proposal will be successful, this certainly will be known well in advance of the decisions about *Kepler*. The value of these *Spitzer* microlensing observations would be greatly augmented by adding targets that were observed by *Kepler* in the 16-29 Apr 2014 window and were in decline at the time of the *Spitzer* window. While this *Kepler* window is 2-months before the anticipated "Summer 2014" start of the new mode of *Kepler* observations, it does not seem impossible to open up this pre-summer 14-day window, in light of the potential synergy with *Spitzer*.

8 Additional Science

There are three other major science goals, in addition to planet masses, that could achieved with these observations.

First, because *Kepler* is probing a different part of the Einstein ring, it will (in most cases) detect planetary perturbations that are not detected from Earth (and also fail to detect those that are detected from Earth). Hence it will increase the number of detected planets. And like the planets detected from Earth, these will have $\pi_{\rm E}$ and $\theta_{\rm E}$ measurements, and thus mass and distance determinations. We estimate a roughly equal number of such planet detections, i.e., two per year.

Second, *Kepler* will measure the masses and distances of essentially all binary microlensing events discovered from Earth. In these cases, the caustics are so big that *Kepler* will detect binary perturbations from the same events as those detected from Earth. However, because it will probe caustic crossings at a substantially different location in the Einstein ring, it will likely enable complete orbital determinations for all such binaries. Note that this is quite rare for Earth-only observations: Shin et al. (2012, 2013) did this for three cases, but all were exceptionally favorable, being very close to the Sun, with consequent large $\pi_{\rm E}$.

While binaries in general are more easily studied in other ways, this is not true for brown-dwarf (BD) binaries, which are difficult or impossible to detect with other methods, particularly close,

low-mass BD binaries. While BD microlensing binaries are not usually distinguishable from main-sequence binaries, Choi et al. (2012) found two cases in which the systems were so close to us that their parallaxes (and so masses and BD status) could be determined. These proved to extend the previously discovered "minimum binding energy" for BDs to a completely new regime in mass and separation. *Kepler* would be able to pick out the BD binaries in all cases, not just the handful of favorable cases that are currently possible.

Finally, while most single-lens events will not have measured $\theta_{\rm E}$, their parallax measurements alone can yield important science. Han & Gould (1996) showed that the lens mass function could be reconstructed from the ensemble of such measurements. While the mass function of luminous stars is more easily studied photometrically, dark objects (like isolated black holes, neutron stars, and old BDs) will show up only in microlensing surveys, which are sensitive to mass, not light.

9 Pathfinder Mission

We have organized this white paper around the goal of measuring microlens parallaxes for planetary events because these would yield individual masses and distances for the planets and their hosts. We have estimated that two such mass measurements could be made per year. Perhaps another two could be made if *Kepler* succeeds in detecting its own planets. This may not seem like a lot, but in fact in the whole history of microlensing planet searches, there have only been four precise mass measurements for planetary systems. In each of these four cases, fundamental insights emerged (Gaudi et al. 2008; Dong et al. 2009a; Muraki et al. 2011; Batista et al. 2013). But each of these four cases was "extremely favorable" in some way, usually because the lens was close to us. So the sample of mass measurements is highly biased in addition to being small. *Kepler* will measure masses and distance of an unbiased subsample, and so will turn up new surprises.

Moreover, in the future, one would like to *routinely* make mass measurements of *essentially all* microlensing planets. This would be possible if a wide-field camera (like *Kepler*) were placed in solar orbit, so that it could simultaneously observe all microlensing events. We have seen that even in its degraded state, *Kepler* will have no trouble measuring parallaxes for the modest fraction of microlensing events that peak near its observing windows. This means that a much more modest satellite could achieve good results during the entire microlensing season, provided that its science requirements were specifically analyzed. The same, or perhaps another specially purposed satellite could obtain microlens parallaxes for *WFIRST* microlensing.

Much would be learned about design issues for such future missions by a pilot microlensing program with *Kepler*.

Work by AG was supported by NSF grant AST 1103471 and NASA grant NNX12AB99G. KH is supported by a Royal Society Leverhulme Trust Research Fellowship and by grant NPRP-09-476-1-78 from the Qatar National Research Fund (a member of Qatar Foundation).

Batista, V. et al. 2013, ApJ, submitted
Boutreux, T. & Gould, A. 1996, ApJ, 470, 201
Choi, J.-Y. 2013, ApJ, 768, 129
Dong, S. et al. 2009a, ApJ, 695, 970
Dong, S. et al. 2009b, ApJ, 698, 1826
Gaudi, B.S. 2012, ARAA, 50 411
Gaudi, B.S. & Gould, A. 1997, ApJ, 477, 152
Gaudi, B.S. et al. 2008, Science, 319, 927
Gould, A. 1995, ApJ 441, L21
Gould, A. 1999, ApJ 514, 869
Gould, A. & Loeb, A. 1992, ApJ, 396, 104
Gould, A. & Yee J.C. 2012, ApJ, 755, L17
Gould, A. & Yee J.C. 2013, ApJ, 767, 42
Gould, A. et al. 1994, ApJ, 423, L105
Han, C. & Gould, A. 1996, ApJ, 467, 540
Muraki, Y. et al. 2011, ApJ, 741, 22
Shin, I.-G. et al. 2011, ApJ, 735, 85
Shin, I.-G. et al. 2012, ApJ, 755, 91
Yee, J.C. et al. 2012, ApJ, 755, 102
Yoo, J. 2004, ApJ, 603, 139

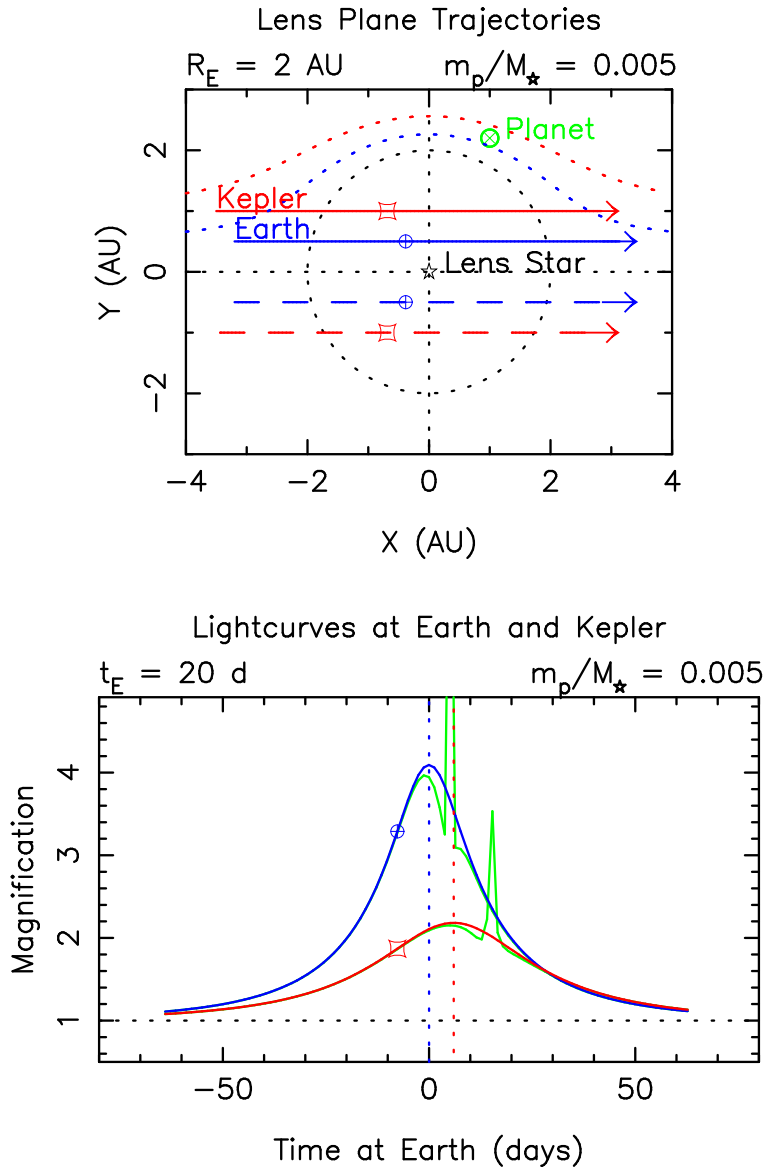

Figure 1: Illustration of four-fold degeneracy derived from comparison of *Kepler* and ground based lightcurves. Upper panel shows two possible trajectories of the source relative to the lens for each of *Kepler* (red) and Earth (blue) observatories. Each set would give rise to the same point-lens lightcurve in the lower panel (same colors), leading to an ambiguity in the Earth-*Kepler* separation (distance between red circle and blue square) relative to the Einstein ring. In this particular case, the planet causes deviations to both lightcurves (green), thus proving that the trajectories are on the same side of the Einstein ring. More generally, the planet would appear in only one curve, leaving the ambiguity open. In this case, it would be resolved by more subtle differences in the Einstein timescale.

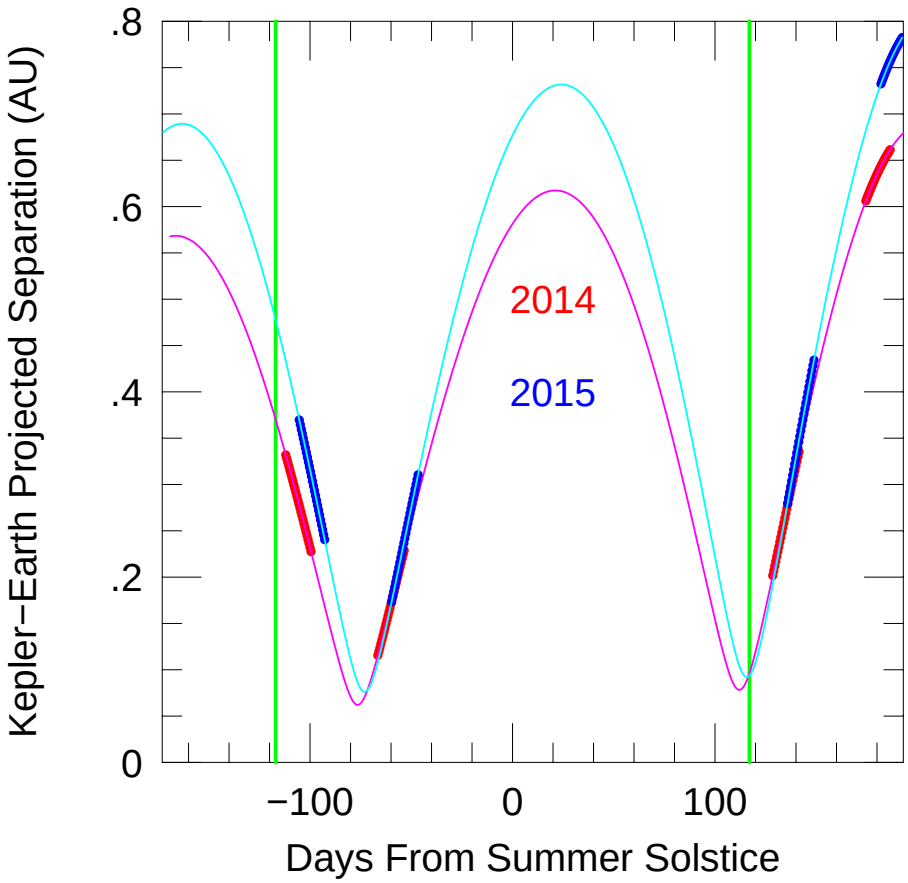

Figure 2: *Kepler*-Earth projected separation in 2014 (magenta line) and 2015 (cyan line) for Galactic Bulge observations. Red and Blue points show the times when the boresight can be pointed ±45° and ±90° from the Sun with the field center still contained within the field of view. Green vertical lines show the approximate boundaries of the microlensing season from Earth.

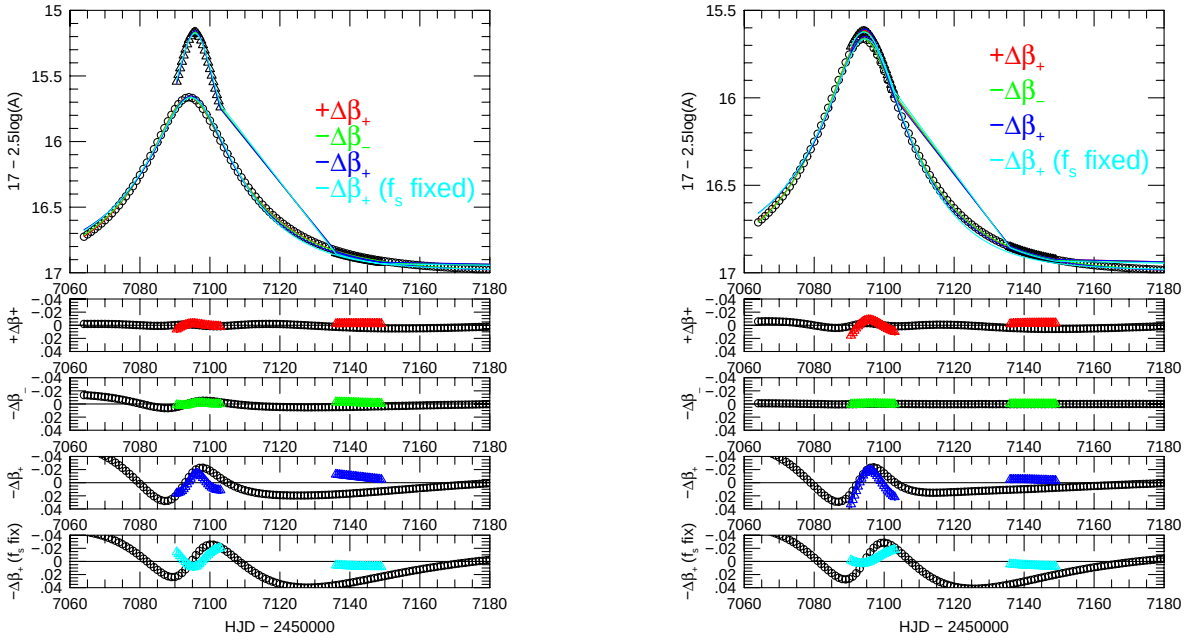

Figure 3: Parallax measurement and degeneracy-breaking for a typical Disk-lens event $(\pi_{E,N}, \pi_{E,E}) = (0.3, 0.3)$ (left) and Bulge-lens event $(\pi_{E,N}, \pi_{E,E}) = (0.03, 0.03)$ (right). Top panels: *Kepler* measurements (triangles) over two 14-day windows and Earth measurements (circles) over much longer timescale both shown on arbitrary magnitude scale. Four different models are shown for each, indicated at right in different colors. (In this panel the model curves overlap and can barely be distinguished). The true model is $+\Delta\beta_-$, i.e., lens passes the source on its right as seen from Earth (+), and Earth/Spitzer both see the lens passing the source on the same side (-). The error bars are 0.005 mag per day from the ground and 0.003 mag per day from *Kepler*. Lower Panels: residuals for each case for Earth (black) and *Kepler* (colored). **Disk (left):** $+\Delta\beta_+$ would have $\pi_E \sim 1.45$ (factor 3.4 too large) but ruled out by $\Delta\chi^2 = 71$; $-\Delta\beta_-$ would have $\pi_E \sim 0.44$ (just 5% too large) and is ruled out by $(\Delta\chi^2 = 71)$. $-\Delta\beta_+$ would have $\pi_E \sim 1.13$ (factor 2.7 too large) and ruled out by $\Delta\chi^2 = 2084$. **Bulge (right):** $+\Delta\beta_+$ would have $\pi_E \sim 1.6$ (factor 38 too large) but ruled out by $\Delta\chi^2 = 147$; $-\Delta\beta_-$ would have $\pi_E \sim 0.048$. This is permitted $(\Delta\chi^2 = 1)$ but it is just 14% too large; $-\Delta\beta_+$ would have $\pi_E \sim 1.13$ (factor 26 too large) and ruled out by $\Delta\chi^2 = 1729$. **Bottom-most panels:** However, all three of these cases allowed for free fitting of F_s. When this is constrained based on technique described in text, the result is shown in the bottom panel for the $-\Delta\beta_+$ case. We then find $\Delta\chi^2 = 3559(vs.\ 2084)$ (disk) and $\Delta\chi^2 = 3636(vs.\ 1729)$ Measurement error is about 0.003 (0.005) in each direction, i.e., $\sim 1\%(15\%)$, but without *Kepler* data, the Earth-based lightcurve would have completely unconstrained parallax (errors of 0.4 in the North direction).